


Novel measurement system for respiratory aerosols and droplets in indoor environments

Michael Lommel¹  | Vera Froese¹ | Moritz Sieber² | Marvin Jentsch² |
Tim Bierewirtz¹ | Ümit Hasirci¹ | Tim Rese¹ | Josef Seefeldt² | Sebastian Schimek² |
Ulrich Kertzscher¹ | Christian Oliver Paschereit²

¹Biofluid Mechanics Laboratory, Institute for Imaging Science and Computational Modelling in Cardiovascular Medicine, Charité – Universitätsmedizin Berlin, Augustenburger Platz 1, Berlin, Berlin 13353, Germany

²Institute of Fluid Dynamics and Technical Acoustics, Hermann-Föttinger-Institute, Chair of Fluid Dynamics, TU Berlin, Straße des 17. Juni, 135, Berlin, Berlin 10623, Germany

Correspondence

Michael Lommel, Biofluid Mechanics Laboratory, Institute for Imaging Science and Computational Modelling in Cardiovascular Medicine, Charité – Universitätsmedizin Berlin, Berlin, Germany.
Email: michael.lommel@charite.de

Abstract

The SARS-CoV-2 pandemic has created a great demand for a better understanding of the spread of viruses in indoor environments. A novel measurement system consisting of one portable aerosol-emitting mannequin (emitter) and a number of portable aerosol-absorbing mannequins (recipients) was developed that can measure the spread of aerosols and droplets that potentially contain infectious viruses. The emission of the virus from a human is simulated by using tracer particles solved in water. The recipients inhale the aerosols and droplets and quantify the level of solved tracer particles in their artificial lungs simultaneously over time. The mobile system can be arranged in a large variety of spreading scenarios in indoor environments and allows for quantification of the infection probability due to airborne virus spreading. This study shows the accuracy of the new measurement system and its ability to compare aerosol reduction measures such as regular ventilation or the use of a room air purifier.

KEYWORDS

aerosol, infection transmission, measurement system, respiratory droplets, virus spread

1 | INTRODUCTION

The SARS-CoV-2 virus is transmitted between humans via aerosols and droplets that are expelled during breathing, talking, sneezing, and coughing. Indoor environments are especially known for their high risk of infection transmission.¹ Respiratory aerosols and droplets disperse in the room, shrink due to evaporation, and remain suspended in the air for several hours. The risk of airborne infection strongly depends on the amount and the duration of time in which an individual is exposed to the virus load. Thus, the analysis of the properties and behavior of the virus in the air are of great interest and the spread of airborne infectious particles in indoor environments has

been the subject of several research studies.^{1–7} While the virus size is approximately 100 nm and the mass is around 1 fg, the respiratory aerosol and droplet distribution emitted during breathing, talking, sneezing, and coughing is in the range of 0.3–100 µm.

Sputum consists of 94.5% water, 0.9% sodium chloride (NaCl), and 4.6% carbohydrate, protein, lipids, and DNA.⁸ Therefore, respiratory droplets and aerosols evaporate slower than pure water droplets and result in solid droplet nuclei of approximately 30% of their original diameter.^{3,4,9,10} Respiratory viruses are embedded and distributed homogeneously in this nuclei.¹⁰

After the emission, droplets and aerosols behave differently depending on their mass. Larger droplets (>100 µm) settle to the

Michael Lommel and Vera Froese should be considered joint first author.

This is an open access article under the terms of the Creative Commons Attribution-NonCommercial-NoDerivs License, which permits use and distribution in any medium, provided the original work is properly cited, the use is non-commercial and no modifications or adaptations are made.

© 2021 The Authors. *Indoor Air* published by John Wiley & Sons Ltd.

ground within a shorter time due to gravity. The middle-sized (20–100 μm) and smaller droplets (5–20 μm), as well as aerosols (<5 μm), remain airborne over a longer period of time and evaporate quickly, depending on environmental conditions like humidity or temperature and their initial diameter.^{2,3,5–7} The evaporation time of aerosols with an initial diameter of 1 μm is 1–2 ms; for small droplets of 10 μm , it is 250–550 ms; and for large droplets of 100 μm , it is 5–30 s.^{3,7,9} After evaporation, the average size distribution of the solid droplet nuclei of sputum is 0.0786–26.2 μm^4 and can linger in still air for 20–60 min.⁶

Because of the higher mass of large- and middle-sized droplets, the resulting viral load is significantly higher than in aerosols and small droplets. Additionally, there is an increased chance of survival for viruses of this magnitude.^{9–11} Thus, after evaporation, the originally middle-sized droplets become small, high-risk droplet nuclei, carrying a great number of active viruses.^{4,10} In their review, Mao et al.⁴ combine this finding with studies on the deposition probability as a function of aerosol size in the upper respiratory tract and the alveolar region.^{12–17} They conclude that aerosols and droplets with a size of 2–10 μm carry the highest risk of infection. Therefore, it is important to investigate aerosol and droplet dispersion at these orders of magnitude, which are mostly responsible for infectious transmissions.

Especially in scenarios with poor ventilation, the ambient air can become enriched with viruses up to a critical concentration. All persons in the environment are simultaneously exposed to a high concentration of viruses and the risk of so-called super-spreading events emerges. Currently, there are no experimental studies that quantitatively determine viral spreading in everyday environments. Most studies use particle size analyzers to evaluate the dispersion and spread of aerosols and droplets in rooms. Noti et al.⁵ measured the spread of viruses in an Aerosol Exposure Simulation Chamber using a breathing and a coughing simulator. They used Madin-Darby canine kidney cells and influenza viruses to determine the influence of air humidity on the risk of infection. The amount of infectious viruses was determined by real-time qPCR analysis and a viral plaque assay (VPA). In another study, Lindsley et al.¹⁸ examined the efficiency of a face shield as protective equipment in the same scenario. The measuring method is very well suited for the direct measurement of virus spread via aerosols. Alsved et al.¹⁹ determined the size of the aerosols and droplets during singing and talking by using this method. However, measurements with a particle size analyzer are limited to a determined range of droplet and aerosol sizes. Moreover, the direct measurement of the virus spread or aerosol and droplet measurements with a particle size analyzer can only be done with much effort in clean room environments. Thus, these measurements are not applicable in everyday environments.

Another important factor is the experimental substitute for sputum, which is used to track the aerosol spread. Most studies use water as a single component droplet model to analyze the evaporation and dispersion.^{2,19–22} However, as stated above, the composition of sputum is much more complex than that of pure water

Practical Implications

- Novel mobile measurement system for the quantitative determination of aerosol and droplet transmission between humans in everyday situations.
- Examination of the effects of protective measures like active or passive ventilation.
- Validation tool for flow simulations of aerosol and droplet dispersion: simultaneous measurement at different positions in the environment.

and the evaporation differs strongly.^{4,5,8} Another substitute that has been used in experimental studies is NaCl-water solution.^{3,7,9} Although the evaporation time of NaCl-water droplets is more similar to water than to sputum, the resulting droplets and aerosols also shrink to a solid nuclei that stays airborne.^{9,23}

To consider and investigate a larger range of parameters that influence the spread of aerosols and droplets, several studies simulate the dispersion of droplets in closed rooms numerically.^{2,6,7,9,24} The simulations allow for the analysis of the aerosol dispersion at any time and position in a room. Important parameters like the velocity during exhalation, humidity, temperature, ventilation pattern or droplet nuclei size (solid phase in the aerosol or droplet), and ventilation rate can be included.²

Nevertheless, a limitation of these simulations is that the airflow in a specific room is influenced by many factors like ventilation slits or door and window columns that cannot be covered by simplified boundary conditions in the simulation.⁹ In most studies, the background flow is solely driven by coughing or sneezing or by defined ventilation. Additionally, turbulent fluctuations are not considered at all or only in a limited way. Therefore, it is necessary to validate the simulation results with experimental measurements.

This study presents an experimental measurement method, which is suitable to measure the spread of aerosols in everyday situations and reproduce the spread of viruses between humans. For this purpose, an emitter was developed that simulates the human droplet and aerosol emission. It releases a NaCl-water solution. The NaCl serves as a tracer embedded in small- and middle-sized droplets or aerosols that evaporate, while the NaCl nuclei remain in the air and follow the room airflow. The size of the NaCl nuclei is in the range of the size of the sputum nuclei after evaporation. Additionally, recipients were developed which simulate inhaling persons at several positions in different spreading scenarios. They are able to quantify the amount of inhaled tracer over time. Thus, the measurement method simulates the tracer inhalation simultaneously at several positions in a specific scenario. It allows for the evaluation of various protective measures like passive or active ventilation or the variation of distances between the emitting and the absorbing persons. The aim of this study was the experimental and analytical validation of the novel measurement method. To validate the measuring results,

an analytical model was set up which calculates the time-dependent concentration of droplets and aerosol depending on the distance to the emitter. The model was also used to determine the effect of the emission mode on the measurement results. In addition, a field study was conducted to demonstrate the suitability of the new system to measure the effect of aerosol reduction measures of ventilation and indoor air purification in indoor environments.

2 | MATERIALS AND METHODS

The setup of the aerosol measurement system consists of one portable emitter and a number of portable recipients that can be positioned in different spatial arrangements with respect to one another. The system is designed to measure the transmission of tracer particles in aerosols and droplets from the emitter to the recipients and to evaluate and compare the infection risk of different configurations with and without protective measures.

2.1 | Emitter

The emitter developed for this study enables the repeatable emission of aerosols and droplets. A siphon fed two-fluid nozzle (XA-SR 050; BETE Fog Nozzle, Inc.) is used to disperse the tracer solution into an aerosol and droplet spray. The emitted fluid is a solution of distilled water with a certain amount of NaCl (sodium chloride $\geq 99.5\%$, p.a., ACS, ISO, Carl Roth). During dispersion, the NaCl is released and acts as a tracer particle dissolved in aerosols and droplets or crystallized as a solid nucleus after evaporation. The tracer solution is kept in a water reservoir with a constant liquid level that is aligned with the outlet of the spray nozzle to avoid hydrostatic pressure differences. This prevents a back flow or fluid leaking from the system between the emissions, which would affect the measurement accuracy. Furthermore, the tracer solution is placed on a microscale (FC-2000, GRAM Group) to measure the total amount of the emitted fluid.

Through the two channels, compressed air and tracer solution are fed into the nozzle and are mixed at the outlet (Figure 1A). A bypass flow (sheath flow), which is injected through four radial inlets, is integrated and positioned circularly around the nozzle to adjust the exhaled volume of air as well as the momentum of the emitted aerosol. The volume flow through the nozzle and bypass system is controlled independently by pressure regulators (DR021-01-3, Landefeld GmbH, Germany) and solenoid valves (SLP15E4, E.MC Machinery Co., Ltd.). The schematic diagram of the nozzle is shown in Figure 1B. As described in the following chapters, the droplet size distribution and outlet velocity are a function of the mass flow and applied pressure to the nozzle and bypass. An exemplary emission is shown in Figure 2. The emitter can be operated in a pulsed or continuous emission mode. The number and frequency of the emissions and the duration of the pauses in between are set by an in-house built pulse generator. The head of the emitter is 3D-printed from polylactide (PLA). The basic head geometry is obtained from free3d.com.²⁵ It is extended by an elliptical mouth opening with an average surface of a woman's mouth during coughing (3.37 cm^2).²⁶ The nozzle is placed at the back of the head so that the emitted aerosol exits through the mouth (see Figure 1A). Except for the mouth opening, the human appearance of the emitter is only for representative purposes and future studies on face masks.

2.2 | Phase Doppler anemometry

In order to characterize the dependence of emitted aerosols and droplets on the supply pressure and air mass flow, a phase Doppler anemometry (PDA) system (SprayExplorer, Dantec Dynamics GmbH) is used.²⁷ The measurement point of the focused laser beams is placed centered and at a distance of $d = 25 \text{ mm}$ to the mouth opening of the emitter. The laser wavelength measures $\lambda = 514.5 \text{ nm}$. The scattering angle is $\phi = 68^\circ$, and the focal length of the transmitter and receiver yields $f_f = 310 \text{ mm}$. The PDA system is able to detect particle diameters in the range of $1\text{--}150 \mu\text{m}$. Each measurement is conducted until the information of 200 000 particles is collected.

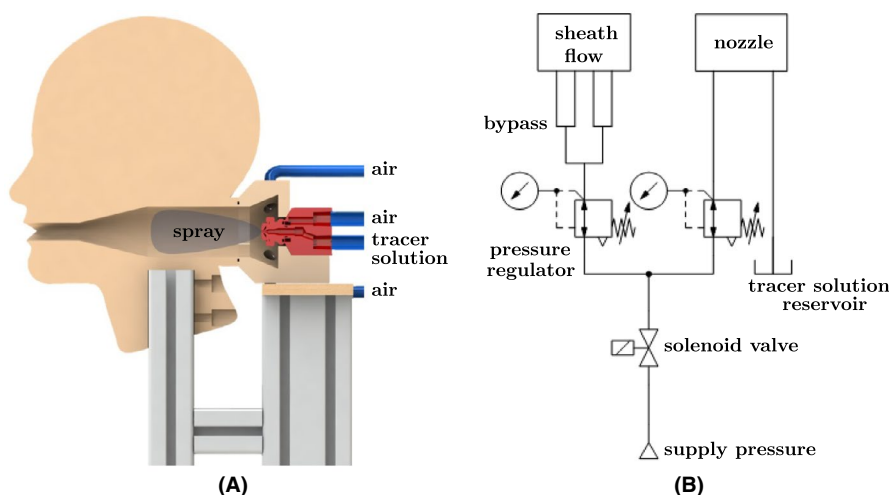


FIGURE 1 (A) The emitter with a two-fluid nozzle. The tracer-fluid-air mixture exits the nozzle as a spray due to the applied pressure. (B) Schematic (P&I) diagram of the emitter

The PDA measurements are conducted with continuous air supply to the nozzle. The supplied air mass flow is controlled using a pressure regulator valve with manometer (DR021-01-3, Landefeld GmbH, Germany) and is monitored using a Coriolis mass flow meter (Promass A, Endress+Hauser AG).

2.3 | Recipients

The aerosol-absorbing recipients (Figure 3) inhale the surrounding air that is enriched with the tracer. The design of the portable recipients is as follows: A vacuum pump (ATTIX 30-01, NILFISK GmbH, Brøndby, Denmark) creates a vacuum in a sealed glass cylinder that is partly filled with 200 ml double deionized water. Due to the vacuum, air with NaCl nuclei, aerosols, or droplets (tracer

particles) is led through a tube (trachea) from the mouth of the face model into the water of the glass cylinder. This part of the recipient is called the water lung. The volume of the aspirating airflow is controlled by two flowmeter sensors (flowmeter DK46, Krohne GmbH) with a variable flow rate of 0 L min⁻¹ to 23.2 L min⁻¹. The inhalation is continuous for the presented investigation. A fine filter paper (Cytiva grade 589/1, Thermo Fisher Scientific) is located at the end of the trachea, completely surrounded by the deionized water. It functions as an atomizer and thus splits the air stream into fine bubbles to dissolve the tracer particles in the water of the glass cylinder, which increases its electrical conductivity. The fluid is pumped continuously by a roller pump (GROTHEN DC 12 V, Aibecy) through a parallel circuit in which the probe of a conductivity meter (HI98192, Hanna Instruments) with a resolution of 0.01 μS and a measure accuracy of ±0.01 μS is implemented. It hereby

FIGURE 2 Image of the emitter as it emits the droplets and aerosols in the scenario of a cough.

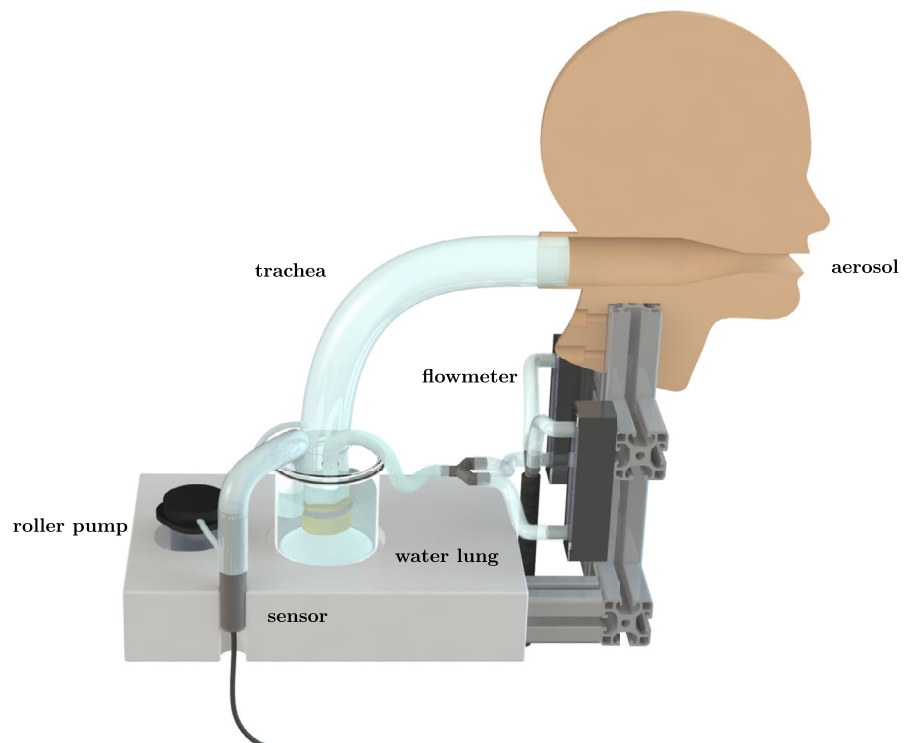


FIGURE 3 Display of a recipient: the aerosol is sucked through the trachea into the water lung by a vacuum. There, a filter dissolves the tracer in the measuring fluid. The measuring fluid is pumped through the sensor by a roller pump. The airflow is adjusted by a flowmeter

measures the increase of the conductivity over time and, thus, the NaCl concentration. These measurement data are used to determine the amount of droplets and aerosols transported from the emitter to the recipient's lungs in relation to the total amount of emitted droplets and aerosols. The face and body of the recipients are used solely for representational purposes and for easier positioning on chairs in a room. The physiological human heat emission can be simulated by heating pads. This influence of the buoyancy effects is not considered in this study to simplify the experimental conditions. This facilitates the repeatability of experimental conditions for the verification of the measurement technique.

2.4 | Measurement procedure

The recipients are placed at defined positions in the room. The frequency and duration of the emission and the inhalation flow rate of the recipients are set. The measurement starts with the recording of the current state: The recipients measure the increase in conductivity without any aerosol emission of the emitter (lead-in time). Thus, in the first minutes of the measurement, the background concentration of particles in the room is measured. This slight increase of the conductivity caused by room specific conductive aerosols or due to aerosols of the previous measurements is possible in every room and has to be eliminated from the actual measurement. Therefore, this background concentration is subtracted as an offset from the measured values during the post-processing. This procedure also shows whether the environment was sufficiently vented after previous measurements. After the lead-in time, the emitter starts exhaling and aerosols and droplets are released in a predetermined amount of ejection cycles (emission period). After the emission stops, the measurement is continued up to a predetermined point in time or until no more increase in conductivity can be measured (lead-out time). During the entire measurement procedure (lead-in, emission, lead-out), the conductivity measurement of each individual recipient is recorded in real time on the measuring device as well as monitored and stored on the measuring computer. The conductivity sensor measures the temperature in the water lung during the entire measurement. The dependence of the conductivity on the temperature is compensated by the device. The room temperature and humidity are recorded accordingly.

2.5 | Verification measurements

To determine the sensitivity, a 0.9% NaCl solution (sodium chloride solution 0.9%, CELLPURE[®], Carl Roth) was pipetted into the measurement system of four recipients. The detectable amount of NaCl was determined by the increase in conductivity.

For the determination of the ability of the water lung to dissolve the tracer from the aspirated air, two water lungs were connected in series. The filter efficiency was determined from the ratio of the increase in conductivity in the two lungs.

The verification measurement for the determination of the measurement accuracy and the comparison with the analytical model was performed in a sealed room at the university with 100 m³ air volume and negligible room air circulation and air exchange rate. Four recipients were positioned around the emitter at a distance of 1.5 m (Figure 4). Due to the specific setup, it was possible to model the dispersion analytically using a spherical model to compare the experimental with the theoretical results (see following paragraph). Moreover, the data obtained from each recipient were compared to the others to determine the accuracy of the measurement method.

The verification measurement followed the measurement procedure stated above. A lead-in time of 300 s was chosen to sufficiently measure the background concentration. The aerosol was released with low momentum (see Table 1) and within an emission period of 500 s with 100 ejection cycles to ensure a good signal to noise ratio. The lead-out time was predetermined to 1300 s. Therefore, the entire measurement time was 2100 s.

A 5% NaCl solution was used as the tracer solution. This particular concentration was selected, because it corresponds to the size reduction of sputum after evaporation.⁴ It results in a tracer particle size of 29% of the original droplet diameter after evaporation, which results from the proportion of the solid phase. The density of 2.16 kg m⁻³ of the salt spheres is higher than the density of the remaining sputum nuclei which consists of further components with lower density like proteins, lipids, carbohydrates, and DNA.⁹ The duration of one cycle of exhalation was set to 2.5 s with a pause of 2.5 s. Thus, the exhalation to pause ratio was 1:1. The inhalation flow rate of the recipients was set to the average flow rate during inhalation of 15 l min⁻¹. The measurement was repeated four times. Between the measurements, the room air was fully ventilated until the conductivity did not further increase and the background concentration of particles was detected anew for each measurement.

2.6 | System response to aerosol reduction measures

To further evaluate the new system and to verify its responsiveness to the aerosol reduction measures venting and room air purification, a field study was conducted. The measurements were performed in a conference room with a volume of 100 m³ and two windows (3 m² opening area) on one side of the room (see Figure 4). During the measurement procedures, the room was fully closed with sealed windows and doors to minimize the air exchange rate. The approach was the same as described in the measurement procedure and verification measurements. Settings of the emitter, recipients, positioning, lead-in time (300 s), emission period (500 s with 100 ejection cycles), and lead-out time (1300 s) were performed accordingly. Three different measures were conducted, and each measurement was repeated three times:

- A measurement without any aerosol-reducing mechanisms.

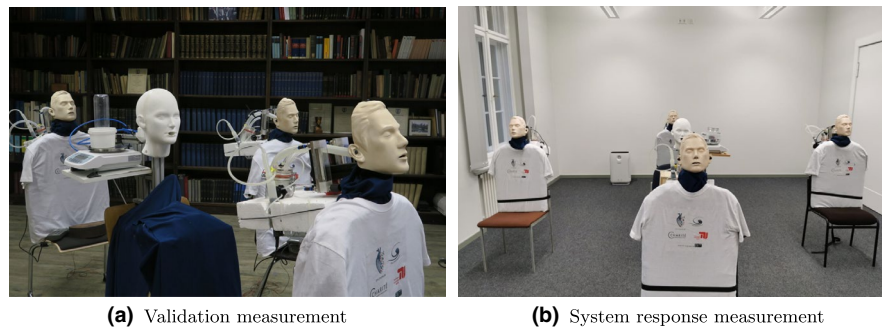


FIGURE 4 Image of the setup and schematic of the positioning in the verification measurement (A) and of the setup in the measurements with ventilation and room air purification (B). In both scenarios, the transmitter is positioned in the center of the four recipients, each of which is located at a distance of 1.5 m from the emitter. At the end of the conference room (B) is the room air purifier.

TABLE 1 PDA parameters and mean results

Pressure [bar]	Mass flow [kg h ⁻¹]	Average diameter [μm]	Average diameter after evaporation [μm]	$D_{(4,3)}$ [μm]	$D_{(4,3)}$ after evaporation [μm]	Velocity [m s ⁻¹]
0.38	0.84	4.37	1.27	35.02	10.16	1.48
0.95	1.41	3.29	0.95	13.89	4.03	2.55
1.65	2.0	2.87	0.83	9.31	2.70	3.52
2.4	2.6	2.52	0.73	8.75	2.54	4.38

Abbreviation: PDA, phase Doppler anemometry.

- A measurement by using a room air purifier (Philips AC2882/10) with HEPA filter. The device was positioned centrally near one wall, that has no windows or doors, at a distance of 3 m from the emitter. It was started at the beginning of the lead-in time with an air exchange rate of 333 m³ h⁻¹.
- A measurement with ventilation. The room was ventilated by opening both windows two times for 120 s after 480 s and 800 s after the beginning of the measurement.

2.7 | Particle migration modeling

The aerosol propagation and the increase of tracer concentration in the air during the verification measurements were investigated analytically. A simplified model was chosen without taking convective transport into account, which was negligible in the verification measurements. The model is utilized to validate the time-dependent aerosol absorption of the recipients and to evaluate the influence of different emission modes, distances between the emitter and the recipients, and different measurement duration of the experimental setup. Therefore, it provides a basis for the generalization of the measured aerosol transmission beyond a specific investigated scenario.

The transport of aerosols and droplets in the air is modeled by diffusion and dissipation in a spherical coordinate system. The spatio-temporal distribution of the aerosol concentration is described by the following differential equation

$$\frac{\partial c}{\partial t} = \frac{v}{r} \frac{\partial^2}{\partial r^2} (Cr) - \mu c, \quad (1)$$

where c denotes the concentration, v the diffusion rate, and μ the dissipation rate. The equation describes the diffusion in spherical coordinates assuming a perfect rotational symmetry. The radius r denotes the distance from the emitter located at the origin. The diffusion process approximates the dispersion of aerosols due to turbulent mixing and molecular diffusion. The dissipation approximates the dilution due to air exchange and settlement of aerosols on the ground.

The equation is approximated in space by a second-order finite difference scheme, and the propagation in time is exactly solved by an exponential integrator of the discretized system. To avoid singularities at the origin, the system is solved for the variable $\tilde{c} = cr$.

The scaling of the absorbed concentration with increasing distance is further characterized by the protection factor (PF), which is given as²⁸

$$PF(r) = \frac{\int_{t_0}^{t_1} c(r_0, t) dt}{\int_{t_0}^{t_1} c(r, t) dt}. \quad (2)$$

It indicates the possible reduction of absorbed aerosols over time at any point r in relation to the point of emission r_0 . Accordingly, a PF of two indicates half the amount of absorbed aerosols.

The diffusion and dissipation equation (1) is simulated in a domain from $r = 0.01$ m to $r = 15$ m for 1800 s, where (aerosol) concentration is added to the domain at the origin with a constant rate for the first 500 s. The grid is refined up to the point in which changes in the simulated concentrations were below 1%. This results in 600 grid points for the simulated conditions. The diffusion rate is varied in the range of $v = 0.001$ m² s⁻¹ to 0.01 m² s⁻¹, which is two orders of magnitude larger than typical molecular diffusion rates in air at normal

conditions. Therefore, the values of the diffusion rate, which are adjusted to replicate the time series observed in measurements, correspond mainly to turbulent diffusion. The dissipation rate is varied in the range of $\mu = 0.0001 \text{ s}^{-1}$ to 0.1 s^{-1} which corresponds to a halving of the concentration in two hours and one minute, respectively.

The experimental results were compared against the analytical model. Therefore, the model was simulated in a sphere of 3 m radius to approximate the volume of the investigated room. The diffusion rate and dissipation rate of the model were calibrated to minimize the sum of squared differences between measurement and simulation. A delay of 10 s in the measurement signal is considered that accounts for the measuring delay of the recipients. For each recipient, the analytical model is compared with the measurement results averaged over the four repetitions and normalized to the maximum conductivity for each case.

3 | RESULTS

3.1 | Aerosol characterization

With the two-fluid nozzle, a wide range of output possibilities could be achieved by varying the parameters (see Appendix 1). It was possible to create aerosol emission conditions similar to those of breathing, talking, sneezing, and coughing. The bypass flow allows high ejection speeds such as sneezing and coughing. The aerosol output with low momentum for breathing and speaking can be simulated without bypass flow. The mass flow, average size, and velocity emission can be adjusted by the pressure applied to the nozzle. With an increasing pressure head of the air, the volume flow and the velocity increase, while the average particle size distribution shifts to smaller particle diameters. A summary of the investigated parameters and the results of the PDA measurements is given in Table 1.

An average diameter of 2.52–4.37 μm was measured. The De Brouckere mean diameter ($D_{(4,3)}$), the mean of the particle size distribution weighted by the volume, was 8.75–35.02 μm for the tested parameters. Furthermore, a mass flow of 0.84 kg h^{-1} to 2.6 kg h^{-1} and a velocity of 1.48 m s^{-1} to 4.38 m s^{-1} of the aerosols and droplets were measured without the bypass flow. Figure 5 shows the relative droplet and aerosol size distribution in relation to the

particle number and aerosol volume percentage of the verification measurement. The pressure was set to 1.65 bar, resulting in a mass flow of 2 kg h^{-1} , a velocity of 3.52 m s^{-1} , and an average diameter of 2.87 μm . The resulting $D_{(4,3)}$ for this configuration was 9.31 μm . After evaporation, the calculated remaining average tracer particle diameter was 0.83 μm and $D_{(4,3)}$ was 2.7 μm .

3.2 | Measurement accuracy and experimental results of the verification measurement

The encoder resolution of the conductivity meter was 0.01 μS . Thus, the smallest increase detectable by the device corresponds to 2.113 μg ($\pm 0.11 \mu\text{g}$) per 0.01 μS . The detection limit of a 5% tracer solution in the water lung is 40.9 μL . This corresponds to $\approx 78\,000$ droplets with a diameter of 10 μm . A filter efficiency of 97.38% ($\pm 0.97\%$) was determined with the measurement of the conductivity increases of two water lungs connected in series.

For the determination of the measurement accuracy, four measurements with four recipients were performed in a room with negligible air convection. After a lead-in time of 300 s, the emission started for 800 s (100 exhalations, emission 2.5 s, pause 2.5 s, ratio 1:1), followed by a lead-out time of 1300 s. The overall sampling duration was 2100 s. An aerosol and droplet quantity of $6.36 \text{ g} \pm 0.38 \text{ g}$ was emitted. Thus, for each measured increase in value (0.01 μS), an average of 0.0033% of the overall amount of tracer particles released within a single exhalation could be detected. The ratio of the power of the signal to the power of the background noise (signal to noise ratio) in this setup was 7.95 (± 0.922). The temperature was $20^\circ\text{C} \pm 1^\circ\text{C}$, and the humidity was 36 ($\pm 2\%$). The average increase in conductivity of the four verification measurements is shown in Figure 6. In this figure, the background concentration during the lead-in time is shown. This concentration increase is always subtracted from the overall increase in post-processing.

During the lead-in time, a slight increase in conductivity was measured. At 300 s, the aerosol emission was started. With a delay of ≈ 300 s, the tracer absorption of the recipients in 1.5 m distance increased over time. At 800 s, the aerosol emission was stopped. In the lead-out time, the tracer particle absorption increased further over time. 350–400 s after the emission was stopped, an inflection

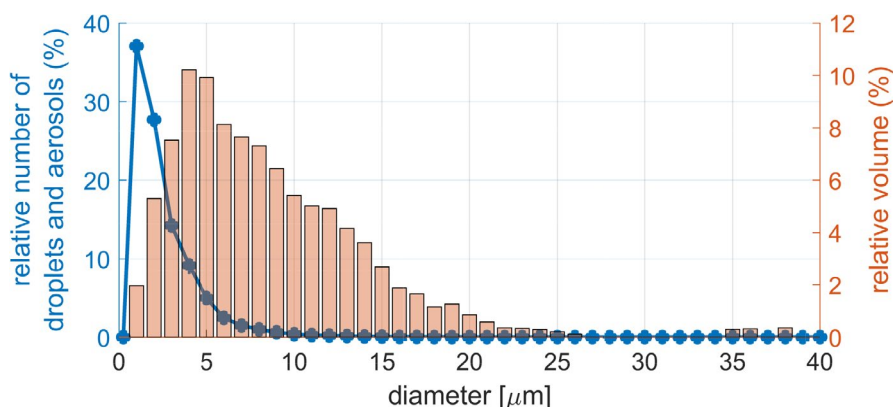


FIGURE 5 Spray characterization in the verification measurement at a pressure of 1.65 bar and mass flow of 2.0 kg h^{-1}

FIGURE 6 Average increase in conductivity for four verification measurements within the same setup: mean values of four recipients, negligible airflow, distance 1.5 m, lead-in time: 300 s, aerosol emission until 800 s, lead-out time 1300 s, and overall sampling duration 2100 s. The dashed lines for each measurement represent the basic increase during the lead-in, which are subtracted from the measurement results in the post-processing

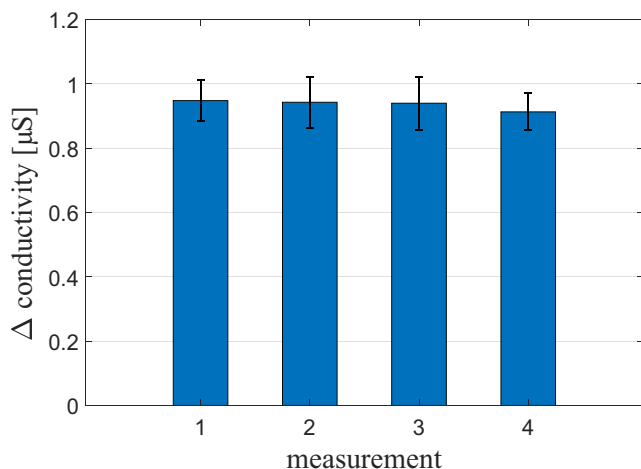
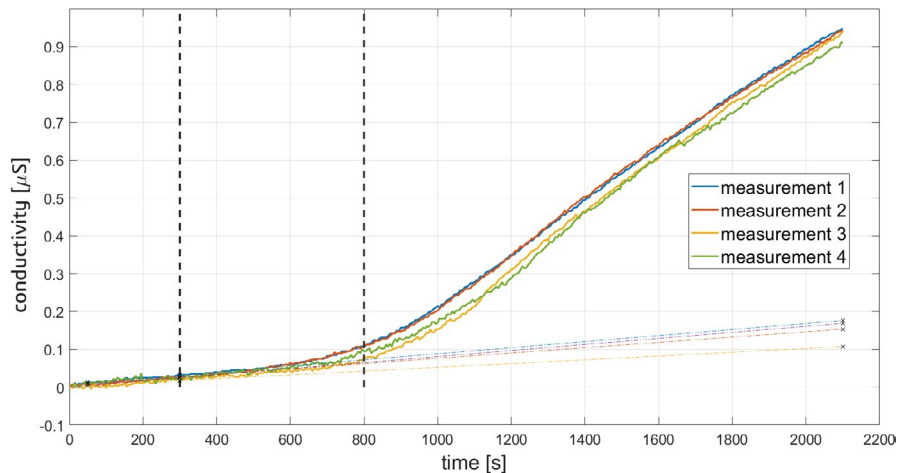


FIGURE 7 Verification measurements: the overall average increase in conductivity after a sampling duration of 2100 s and the standard deviation of the four recipients is shown. Four measurements with four recipients were performed. The distance between the recipients and the emitter was 1.5 m. As tracer solution a 5% NaCl solution was used. A total of 100 exhalations with a duration of 2.5 s and a pause of 2.5 s were performed, during which a total of $6.36 \text{ g} \pm 0.38 \text{ g}$ tracer solution was emitted. Thus, the exhalation to pause ratio was 1:1

occurred and the tracer absorption decreased slightly over time until the end of the measurement. The overall average increase over the four experiments is $0.936 \text{ } \mu\text{S}$ with a standard deviation of $\pm 1.46\%$. This increase in conductivity refers to an absorbed tracer solution mass of 198, which corresponds to 0.003% of the overall emitted aerosol. The measurement accuracy among the four recipients within a single experiment was $\pm 7\%$ (Figure 7).

3.3 | Analytical modeling of aerosol dispersion

The time series at selected conditions is displayed in Figure 8 indicating several characteristics of the investigated problem. It is visible that the start of concentration increase and the decay after stopping the emission are delayed, depending mainly on the diffusion rate. The maximum of the observed concentration scales directly with

the diffusion rate and inversely with the dissipation rate. For large dissipation rates, steady-state conditions can be reached, where the concentration approaches a constant value during the emission. Similarly, a complete decay of the concentration in the investigated time frame is only observed for large dissipation rates.

To further describe the scaling of the absorbed concentration with an increasing distance, the PF (2) is computed for the entire simulation time ($t_0 = 0 \text{ s}$ and $t_1 = 1800 \text{ s}$, see Figure 8). The scaling of the PF is found to be exponential with the distance as indicated in Figure 9A. To relate this exponential trend to the simulation parameters, the radial dependency is approximated by an exponential function

$$\text{PF}(r) \approx \exp(\alpha r) \quad (3)$$

in the range from $r = 1 \text{ m}$ to $r = 5 \text{ m}$. The PF scaling exponent α is found to be almost perfectly proportional to $\sqrt{\mu/v}$ as displayed in Figure 9B. The observed deviations from this proportionality are related to very low dissipation rates $\mu < 0.001 \text{ s}^{-1}$, where the simulated time is too short to account for the slow time scale of the dissipation process. The increase of the simulation time (not displayed) collapses all the points to a straight line.

The PF and the related scaling exponent are found to be independent of the emission duration and magnitude, given that the observed time frame is long enough to capture the time scale of the process. The same proportionality is found if a short impulsive emission at the beginning is considered or a continuous emission for the entire observation time. The investigations show that no matter how the aerosol emission is timed and how much aerosol is emitted, the relative decrease of aerosol inhalation with distance is always the same, given that the observation time is long enough. However, the absolute amount of inhaled aerosol strongly depends on the emission mode and the duration of the exposure.

3.4 | Agreement of the verification measurement with the analytical model

An excellent agreement could be found between the verification measurement and the analytical model. Two exemplary graphs are shown in Figure 10. The calibrated model parameters for the four

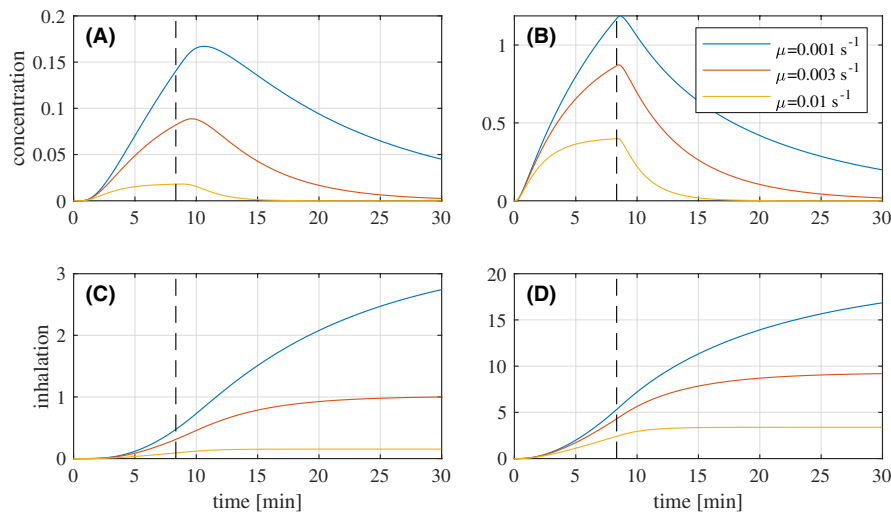


FIGURE 8 Simulated time series displayed at a distance of $r = 1 \text{ m}$ from the origin for discussion rates $v = 0.001 \text{ m}^2 \text{ s}^{-1}$ (A and C) and $v = 0.01 \text{ m}^2 \text{ s}^{-1}$ (B and D). The graphs (A) and (B) show concentration for different dissipation rates μ . The graphs (C) and (D) display the integral of the concentration given in graphs (A) and (B), respectively, which is measured in the experiments as the increase of the conductivity. The dashed vertical line indicates the stopping time of the emission.

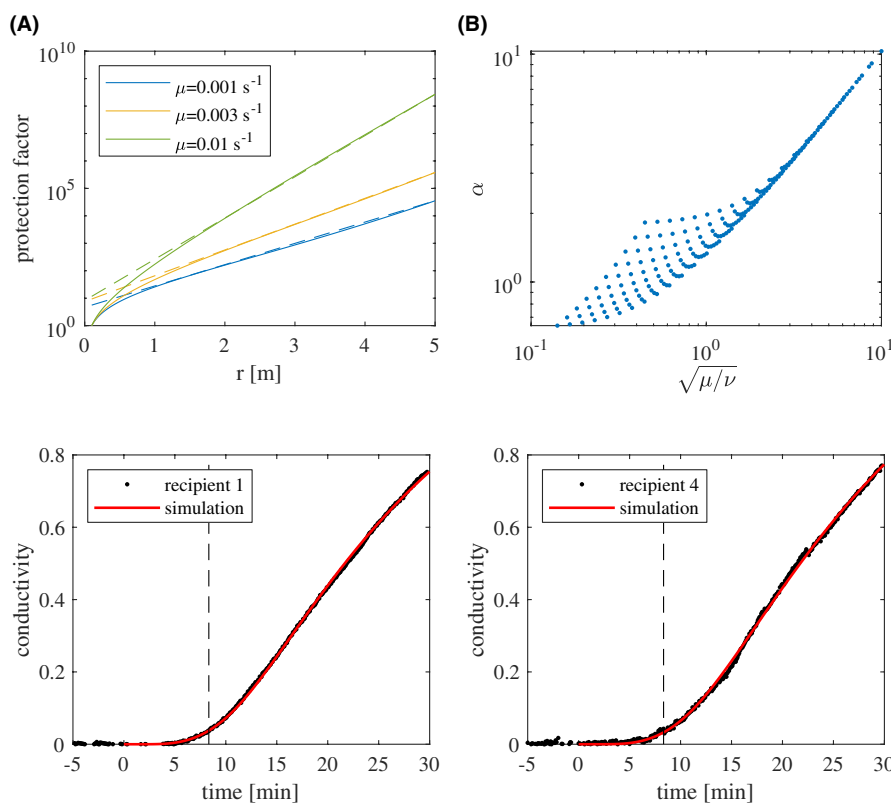


FIGURE 9 (A) Protection factor (PF) at selected conditions and the approximated exponential trend indicated by the dashed lines. (B) The exponential scaling of the $\text{PF}(r) \approx \exp(\alpha r)$ is displayed for all simulated conditions (diffusion rate $v = 0.001 \text{ m}^2 \text{ s}^{-1}$ to $0.01 \text{ m}^2 \text{ s}^{-1}$ and dissipation rate $\mu = 0.0001 \text{ s}^{-1}$ to 0.1 s^{-1}).

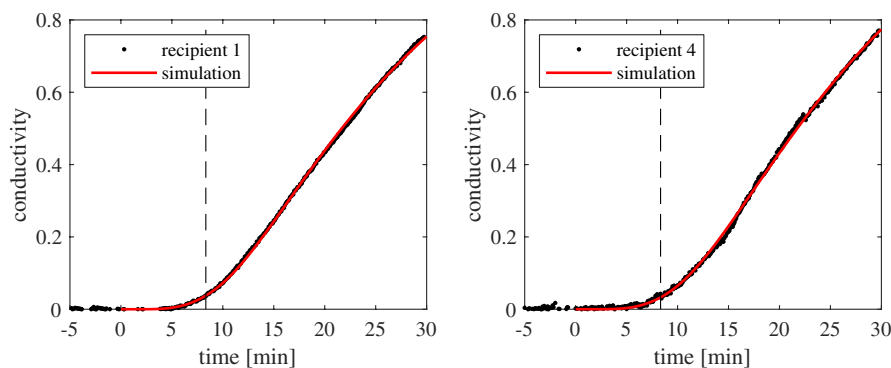


FIGURE 10 Verification measurements and simulation results calibrated to the measured curves.

recipients are presented in Table 2. Among the four recipients, the average diffusion rate is $0.647 \times 10^{-3} \text{ m}^2 \text{ s}^{-1}$ ($\pm 0.052 \times 10^{-3} \text{ m}^2 \text{ s}^{-1}$). The average dissipation rate is $0.9125 \times 10^{-3} \text{ m}^2 \text{ s}^{-1}$ ($\pm 0.087 \times 10^{-3} \text{ m}^2 \text{ s}^{-1}$). Thus, both show a standard deviation of $<10\%$.

3.5 | Response of the system to ventilation and air purifying

Two different aerosol reduction measures were compared to a reference measurement without any measures in the same room (see Figure 11). All three measurements were repeated three times with four recipients, respectively.

3.5.1 | Reference measurement

The reference measurement showed very similar results and curve progression to the verification measurement described above (see Figure 6). The tracer absorption of the recipients in 1.5 m distance began to increase over time $\approx 300 \text{ s}$ after the emitter was started. In the lead-out time (after 800 s), the tracer particle absorption increased further over time. The curve showed a slight turning point $350\text{--}400 \text{ s}$ after the emission was stopped, and the tracer absorption decreased slightly over time until the end of the measurement.

The overall average increase over the three experiments in the measurement without any measures was $0.76 \mu\text{S}$ with a

standard deviation of 1.87%. This increase in conductivity refers to an absorbed tracer solution mass of 160.16 μg . The temperature was $17.7^\circ\text{C} \pm 1^\circ\text{C}$, and the humidity was 35% (2%).

3.5.2 | Air purifier measurement

During the emission period (300–800 s), the aerosol absorption with the air purifier increased significantly faster, than within the other two measurements. During the emission phase, a strong increase of the conductivity and thus the aerosol absorption could be measured. After stopping the emitter, a turning point occurred and the aerosol concentration in the room continued to be lowered and the slope of the curve is decreasing until the end of the measurement. Overall, it provided a fundamentally lower increase in the absorption curve up to 0.53 μS with a standard deviation of $\pm 9.27\%$ over the three experiments. Thus, an average mass of 112.04 μg of the tracer solution has been absorbed, which is 30% less than without any measures. The temperature during the three repeated experiments was $17.5^\circ\text{C} \pm 1^\circ\text{C}$, and the humidity was 36 ($\pm 2\%$).

TABLE 2 Results of the diffusion rate and dissipation rate for the model calibration

Recipient number	Diffusion rate v [$\text{m}^2 \text{s}^{-1}$]	Dissipation rate μ [s^{-1}]
1	0.640×10^{-3}	1.016×10^{-3}
2	0.732×10^{-3}	0.927×10^{-3}
3	0.623×10^{-3}	0.775×10^{-3}
4	0.594×10^{-3}	0.932×10^{-3}

3.5.3 | Ventilation measurement

In the beginning of the emission of the ventilation measurement (from 300 s to 480 s), almost no increase of conductivity could be measured. This equals the curve progression of the measurement without any measures. About halfway of the first ventilation 480–600 s, the aerosol absorption suddenly increases sharply. Subsequently, while the windows were closed and the emitter was still generating aerosol (after 600–800 s), a similar increase as in the measurement with the room air purifier occurred. During the second ventilation from 800 s to 920 s, the emission phase is already over and the curve flattens. Accordingly, a flatter curve with a lower aerosol uptake compared to the reference measurement can be observed thereafter. The concentration in the room remained almost constant and decreased only very slightly over time. Thus, the recipients continued to absorb a constant amount of aerosol. The overall average increase over the three experiments in this measurement was 0.51 μS with a standard deviation of 2.8%. After 2100 s, a solution mass of 106.77 μg of the overall emitted aerosol has been absorbed, 33% less than in the measurement without any measures. The temperature during the three repeated experiments was $17.6^\circ\text{C} \pm 1.5^\circ\text{C}$, and the humidity was 36 ($\pm 2\%$).

4 | DISCUSSION AND LIMITATIONS

4.1 | Verification of the novel measurement system

The novel measurement system enables the quantification of the spread of tracer particles in aerosols and droplets in indoor environments. Due to the high sensitivity and low measurement fluctuations, the system can detect small amounts of aerosol (40.9 nl of a

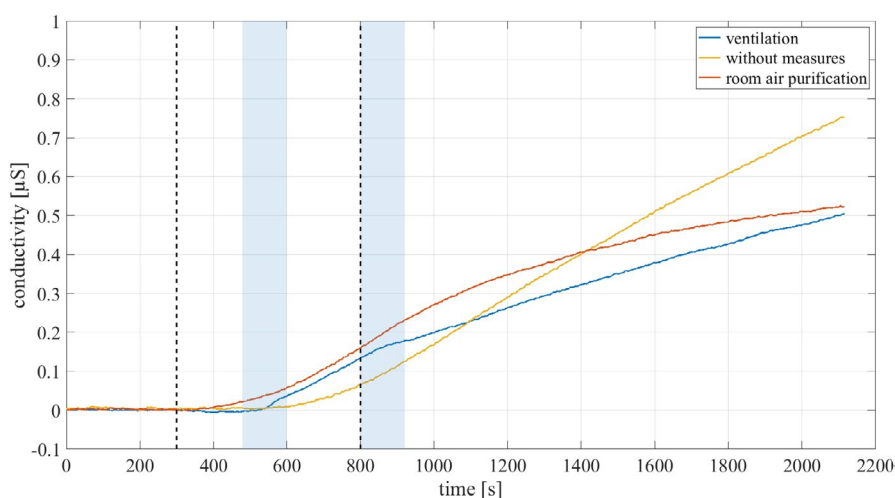


FIGURE 11 The overall average increase in conductivity after a sampling duration of 2100 s is shown. The dashed vertical lines mark the start 300 s and end 800 s of aerosol emission of each measurement. Each curve is based on three measurements with four recipients, respectively. The yellow curve represents the measurement with no aerosol-reducing measures. The measurement shown by the red curve has been conducted with a room air purifier, filtering the air with a HEPA filter from the start to the end of the measurement. During the ventilation measurement (blue curve), the room was ventilated two times (after 480 s and 800 s) for 120 s (blue highlighted sections).

5% tracer solution per measurement value of 0.01 μS). A very high measuring accuracy of the average tracer absorption among the four verification experiments could be demonstrated with a standard deviation of only $\pm 1.46\%$. Thus, measurements over long distances with small aerosol quantities are possible. The water lungs are capable of dissolving and detecting 97.38% ($\pm 0.97\%$) of the incoming tracer, which reaches the measurement fluid in form of solid nuclei or in dissolved form in droplets and aerosols.

The system has been compared to an analytical model which provides realistic estimations of how the emission mode effects the results of the measurement. It concludes that if the observation time is long enough, the relative aerosol inhalation with distance is independent of the emission mode. The fitted model shows a diffusion rate and a dissipation rate with time scales in the order of 1×10^{-3} s. This indicates that the measurement duration of 1800 s was chosen long enough to capture all effects sufficiently. However, the absolute amount of inhaled aerosol strongly depends on the emission mode and the duration of the exposure.

The modeling of the aerosol uptake in the verification measurement shows an excellent agreement with the measured values. The modeling of the individual recipients shows a small standard deviation of the diffusion rate and dissipation rate of under $<10\%$. The setup of the analytical model is only a coarse simplification that does not consider convective transport and thermal stratification of the environment, which are both very relevant for everyday environments. Nevertheless, the investigation of Mittal et al.²⁸ shows that even in realistic scenarios with convection and stratification, a simple scaling of the PF can be found.

Most measurement methods only quantify the evaporation and dispersion of aqueous droplets and aerosols.^{2,19-22} However, the liquid part of the aerosols and droplets evaporates in the range of milliseconds to seconds, depending on humidity and temperature.⁴ In this case, dried, potential virus-containing sputum nuclei remain airborne, follow the airflow, and are potentially infectious for hours.^{4,29} Measurement methods that only spread and analyze aqueous droplets neglect this aspect, whereas this novel measuring method is able to reproduce this process due to the applied tracer particles.

The reaction time of the measurement setup is 5–20 s. Changes in the tracer concentration in the recipients' water lungs can be detected with relatively low measuring delay. Thus, during a measurement process, the effect of different changes in the environment like ventilation or air filtration can be quantified in real time.

The size of the tracer nuclei depends on the concentration of the tracer solution. The higher the amount of the tracer concentration, the larger the diameter of the crystals that remain in the air after the water is evaporated.²³ Thus, a concentration should be chosen, which results in droplet nuclei in the same magnitude as the modeled aerosols and droplets after evaporation and increases the conductance in the water lung enough to exceed the measurement noise. Therefore, in environments with very low transmission of aerosols (eg, rooms with strong ventilation), it can be necessary to increase the concentration and the amount of emitted tracer solution. A

tracer solution of 5% was chosen in the measurements, because it creates crystals with sizes in the same order of magnitude (see Figure 3) as the distribution in a human cough after evaporation.⁴

An almost perfect ability to follow the airflow is assumed for all particles smaller than 20 μm after evaporation.³⁰

In the measurements, a higher mass flow is emitted than during speaking. This increases the humidity in the immediate vicinity of the emitter. It is assumed that this does not influence the results of the measurements significantly due to the distance of 1.5 m between emitter and recipients.

In the measurements, the emitted air has not been heated, so the trajectory deviates from body heated exhaled air. In addition, the airflow caused by the plume was not mimicked, so the exposure of the recipient could be underestimated. The error depends on the principle of room air distribution. The errors can be prevented by further improvements of the measurement system. The electrostatic charge of the materials has not been checked. It is therefore possible that charged NaCl particles have deposited on the walls. The aerosol uptake may therefore have been underestimated.

4.2 | The novel measurement system in different indoor environments

In the system response measurements, the measurement without aerosol reduction measures proceeds similar to the verification measurements. With the room air purifier, the aerosol absorption starts earlier, which can be explained by the increased convection of the room air. After the aerosol emission, the aerosol absorption decreases steadily over time, which can be explained by the continuous reduction of the aerosol concentration. This resulted in a 30% reduction in total aerosol absorption over the measurement period. In the ventilation measurement, the first opening also causes convection of the room air and therefore an earlier increase in aerosol absorption. Both ventilation processes caused a reduced slope and therefore a reduced aerosol concentration in the room air. During the periods without ventilation, the aerosol absorption remains almost constant over time, which indicates a constant concentration. The short-term ventilation procedures reduced the total aerosol absorption by 33%. The effect of the measures and the reduction of the total absorption could be recorded repeatably with the novel measuring system. The results are in line with expectations.

As shown in this field study, the new system is able to display changes in the environment such as the opening of windows or the switching on of a room purifier within seconds. It is therefore very well suited for testing various measures to reduce aerosol dispersion in a wide variety of rooms. Instead of applying general safety measures, specific precautions can be tailored toward the risk of infection in different environments. The high fluctuations during ventilation did not influence the system accuracy and the standard deviation was only 2.8%. The increased convection due to the room air purifier resulted in a standard deviation of 9.27%.

A major advantage of the new measurement system with tracer particles is its broad applicability. In contrast to other methods, it is not limited to clean rooms. The measurement can be performed in various scenarios of indoor environments, because it was not disturbed by dirt or dust in any of the environments investigated so far. It is not harmful, since it does not use toxic components, dyes, or laser beams or causes biological contamination like the real-time qPCR methods.⁵ A restriction might only evolve in environments where the air contains a similarly high concentration of conductive particles as the emitted tracer solution. Nonetheless, the background concentration of particles is detected anew for each measurement. If a room has been fully ventilated after a measurement or if there is any background concentration, can be derived by a change of increase of the conductivity in the lead-in time, which than will be subtracted from the overall increase. In Figure 4, in the verification measurement, the increase due to the background concentration is represented by the dashed lines, whereas in the system response measurement (Figure 11), it has already been subtracted from the entire curves respectively. The measurement system is portable and can be placed on seats or chairs in a room, and the positioning can be changed easily within minutes.

In order to obtain the most expressive and comprehensive measurement output possible, the positioning of the recipients in the room or environment of the emitter is essential. Whether a tracer will reach a certain recipient in a certain time mainly depends on the flow field. For the application in rooms with complex airflow, it is therefore helpful to perform a smoke spread analysis³¹ prior to the measurements. This gives a good first impression of the global flow in the room. Afterward, especially critical areas can be analyzed by the emitter and the recipients.

4.3 | Outlook

Currently, the spread of viruses in everyday situations is mainly evaluated by flow simulations. However, the flow simulations make strong simplifications and cannot take the many disturbing influences into account, such as local temperature fluctuations, convection through window gaps and door slits, and evaporation of droplets. Therefore, it is important to validate the results of the simulations. This system is very well suited for this purpose, as it simultaneously delivers time-resolved measurement data at several positions in the environment.

For this study, the human appearance of the recipients and the emitter is for representative purposes and for an easier positioning only. The physiological human heat emission can be simulated in future studies by heating pads. Furthermore, in a current redesign we plan for heating the liquid phase of the aerosol before atomization in order to prevent a temperature drop due to the evaporation. However, the realistic representation of human plume in experimental investigations is beyond the focus of the current paper. The recipients and physiological human breathing differ from each other, since the inhalation of the recipients is continuous. This is sufficient

for the examination of the spreading of aerosols and droplets, as long as a transport of aerosols and droplets mainly driven by large flow structures can be assumed. The local pulsatile flow dynamics due to in- and exhaling processes would not play a significant role in this context. However, for the future potential evaluation of masks, it would be more appropriate to include an inhalation and exhalation rhythm. In this context, the flow dynamics in the direct vicinity of the individuals become more important. The system will be further developed for these applications, and the human appearance will be necessary for a realistic fit of the masks. Medical face masks are currently tested according to the DIN EN standard on requirements and test procedures for medical face masks. Herein, the tests are performed with a particle size of 0.65–7 μm (DIN EN 14683:2019-1). With the emitter, it is possible to generate the corresponding droplet and aerosol distribution and evaluate the masks accordingly.

The system could be suitable to evaluate schools or offices as well as event locations, cinemas or public transport. An individual protection strategy could be developed, and the efficiency of protective measures could be quantified. In addition to the measurements of this study, the measurement system has already been tested in a large concert hall, a train, and a dentist's examination room with promising results. Initial measurements outdoors are also in progress. The results of these additional measurements in indoor and outdoor environments will be presented in future studies.

As long as a representation of airborne salt crystals is valid in terms of size, the model can also be used to recreate and analyze the propagation processes of other bioaerosols like bacteria, fungi, or pollen and aerosols consisting of inorganic harmful substances.

5 | CONCLUSION

The novel measurement system allows for the quantitative determination of aerosol and droplet transmission between humans in everyday situations. Due to its portability, it can be used on-site and measure in real time with a relatively short measurement delay. The experimental in situ characterization allows for the examination of the effects of protective measures like active or passive ventilation and face masks without underlying assumptions or constraints like clean room environments of several other experimental measurement techniques. Moreover, it is a useful tool to validate flow simulations of aerosol and droplet dispersion at different positions in the environment experimentally. The emitter is able to simulate aerosol and droplet emission with the same characteristics as a human during breathing, talking, sneezing, and coughing. The tracer can be measured with a resolution of 40.9 nl of a 5% tracer solution per measurement value. The recipients detect 97.38% ($\pm 0.97\%$) of the incoming tracer. In the verification measurements of this study, a very high measurement accuracy of the average tracer absorption among the four verification experiments was demonstrated with a standard deviation of $\pm 1.46\%$. Thus, the measurement system has proven to be reliable due to its high sensitivity and low measurement fluctuation. This has also

been demonstrated in the system response measurement. The two different measures ventilation and room air purifying could be represented and evaluated very well by the measurements, where both processes were able to reduce aerosol uptake by about one-third after 2100 s. Despite the expected high fluctuations during ventilation, the standard deviation was only 2.8%. In conclusion, this method is suitable to assess the respiratory hazards of everyday situations in private and public indoor environments, enabling the evaluation of ventilation strategies, air purification technologies, and further protective measures.

ACKNOWLEDGMENTS

The valuable and inspiring support of Joshua Gray is gratefully acknowledged.

PEER REVIEW

The peer review history for this article is available at <https://publons.com/publon/10.1111/ina.12860>.

ORCID

Michael Lommel  <https://orcid.org/0000-0003-1788-276X>

REFERENCES

- Qian H, Miao T, Liu L, Zheng X, Luo D, Li Y. Indoor transmission of sars-cov-2. *Indoor Air*. 2020;31(3):639-645.
- Chen C, Zhao B. Some questions on dispersion of human exhaled droplets in ventilation room: answers from numerical investigation. *Indoor Air*. 2009;20(2):95-111.
- Liu L, Wei J, Li Y, Ooi A. Evaporation and dispersion of respiratory droplets from coughing. *Indoor Air*. 2017;27(1):179-190.
- Mao N, An CK, Guo LY, Wang M, Guo L, Guo SR, Long ES. Transmission risk of infectious droplets in physical spreading process at different times: a review. *Environ Res*. 2020;185:188-109819.
- Noti J, Blachere F, McMillen C, et al. High humidity leads to loss of infectious influenza virus from simulated coughs. *PLoS One*. 2013;8(2):e57485.
- Vuorinen V, Aarnio M, Alava M, et al. Modelling aerosol transport and virus exposure with numerical simulations in relation to sars-cov-2 transmission by inhalation indoors. *Saf Sci*. 2020;130:104866.
- Xie X, Li Y, Chwang ATY, Ho PL, Seto WH. How far droplets can move in indoor environments – revisiting the wells evaporation-falling curve. *Indoor Air*. 2007;17(3):211-225.
- Spicer SS, Martinez R. Mucin biosynthesis and secretion in the respiratory tract. *Environ Health Perspect*. 1984;55:193-204.
- Redrow J, Mao S, Celik I, Posada JA, Feng ZG. Modeling the evaporation and dispersion of airborne sputum droplets expelled from a human cough. *Build Environ*. 2011;46(10):2042-2051.
- Vejerano EP, Marr LC. Physicochemical characteristics of evaporating respiratory fluid droplets. *J R Soc Interface*. 2018;15(139):20170939.
- Wei J, Li Y. Enhanced spread of expiratory droplets by turbulence in a cough jet. *Build Environ*. 2015;93:86-96.
- Austin E, Brock J, Wissler E. A model for deposition of stable and unstable aerosols in the human respiratory tract. *Am Ind Hyg Assoc J*. 1979;40(12):1055-1066.
- Gralton J, Tovey E, McLaws M-L, Rawlinson WD. The role of particle size in aerosolised pathogen transmission: a review. *J Infect*. 2011;62(1):1-13.
- Guo L, Johnson GR, Hofmann W, Wang H, Morawska L. Deposition of ambient ultrafine particles in the respiratory tract of children: a novel experimental method and its application. *J Aerosol Sci*. 2020;139:105465.
- Knight V. Viruses as agents of airborne contagion. *Ann N Y Acad Sci*. 1980;353(1):147-156.
- Morrow PE. Physics of airborne particles and their deposition in the lung*. *Ann N Y Acad Sci*. 1980;353(1):71-80.
- Yeh HC, Phalen RF, Raabe OG. Factors influencing the deposition of inhaled particles. *Environ Health Perspect*. 1976;15:147-156.
- Lindsley WG, Noti JD, Blachere FM, Szalajda JV, Beezhold DH. Efficacy of face shields against cough aerosol droplets from a cough simulator. *J Occup Environ Hyg*. 2014;11(8):509-518.
- Alsved M, Matamis A, Bohlin R, et al. Exhaled respiratory particles during singing and talking. *Aerosol Sci Technol*. 2020;54(11):1245-1248.
- Kukkonen J, Vesala T, Kulmala M. The interdependence of evaporation and settling for airborne freely falling droplets. *J Aerosol Sci*. 1989;20(7):749-763.
- Wang Y, Yang Y, Zou Y, Cao Y, Ren X, Li Y. Evaporation and movement of fine water droplets influenced by initial diameter and relative humidity. *Aerosol Air Qual Res*. 2016;16(2):301-313.
- Zhang Y, Feng G, Bi Y, Cai Y, Zhang Z, Cao G. Distribution of droplet aerosols generated by mouth coughing and nose breathing in an air-conditioned room. *Sustain Cities Soc*. 2019;51:101721.
- Majchrzycka K. *Nanoaerosols, Air Filtering and Respiratory Protection: Science and Practice*; London, New York: CRC Press; 2020.
- Lindsley WG, King WP, Thewlis RE, et al. Dispersion and exposure to a cough-generated aerosol in a simulated medical examination room. *Journal of Occupational and Environmental Hygiene*. 2012;9(12):681-690.
- Printable Models. FemaleHead V4 3D-Modell. 2020. <https://free3d.com/3d-model/femalehead-v4--971578.html>
- Gupta JK, Lin C-H, Chen Q. Flow dynamics and characterization of a cough. *Indoor Air*. 2009;19(6):517-525.
- Albrecht H-E, Borys M, Damaschke N, Tropea C. *Laser Doppler and Phase Doppler Measurement Techniques*. Experimental Fluid Mechanics. Berlin and Heidelberg: Springer; 2003.
- Mittal R, Meneveau C, Wu W. A mathematical framework for estimating risk of airborne transmission of covid-19 with application to face mask use and social distancing. *Phys Fluids*. 2020;32(10):101903.
- van Doremalen N, Bushmaker T, Morris DH, et al. Aerosol and surface stability of sars-cov-2 as compared with sars-cov-1. *N Engl J Med*. 2020;382(16):1564-1567.
- Melling A. Tracer particles and seeding for particle image velocimetry. *Meas Sci Technol*. 1997;8(12):1406-1416.
- Kalliomaki P, Saarinen P, Tang J, Koskela H. Airflow patterns through single hinged and sliding doors in hospital isolation rooms. *Int J Vent*. 2015;14:154-168.

How to cite this article: Lommel M, Froese V, Sieber M, et al. Novel measurement system for respiratory aerosols and droplets in indoor environments. *Indoor Air*. 2021;31:1860-1873. <https://doi.org/10.1111/ina.12860>

APPENDIX 1

TABLE A1 CRedit

Author	Conceptualization	Data curation	Formal analysis	Funding acquisition	Investigation	Methodology	Project administration	Resources	Software	Supervision	Validation	Visualization	Writing - original draft	Writing - review and editing
Michael Lommel	x	x	x		x	x	x	x	x	x	x	x	x	x
Vera Froese	x				x	x	x		x			x	x	x
Moritz Sieber	x	x	x		x	x		x			x	x	x	x
Marvin Jentzsch		x	x		x			x				x	x	
Tim Bierewirtz	x					x								
Ümit Hasirci		x			x			x				x		
Tim Rese		x			x			x						
Josef Seefeldt		x			x			x						
Sebastian Schimek	x					x				x			x	
Ulrich Kertzscher	x			x			x	x		x				
Oliver Paschereit	x			x			x			x				